scientific reports

OPEN

Green synthesis of thiourea derivatives from nitrobenzenes using Ni nanoparticles immobilized on triazine-aminopyridine -modified MIL-101(Cr) MOF

Sara Heidari, Sedigheh Alavinia & Ramin Ghorbani-Vaghei ✉

Nanohybrid metal–organic frameworks (MOF) have recently been considered next-generation catalysts regarding their unique features like large surface-to-volume ratio, tailorable geometry, uniform pore sizes, and homogeneous distribution of active sites. In this report, we address the triazine-aminopyridine-modified 3D Cr-centred MOF MIL-101(Cr)-NH$_2$ following a post-synthetic modification approach. The excellent chelating ability of triazine-aminopyridine was applied to immobilize Ni ions over the host matrix MOF. The as-synthesized material was physicochemically characterized using various analytical techniques like FT-IR, electron microscopy, EDS, elemental mapping, XRD, and ICP-OES. Subsequently, the material has been catalytically employed in synthesizing new thiourea derivatives by reacting to nitrobenzene derivatives and phenyl isocyanate. The catalyst was isolated by centrifugation and recycled in 6 consecutive runs without momentous loss of its reactivity.

Numerous studies have been done since MOFs appeared in our world nearly two decades ago, and new studies continue to be done with increasing interest[1–6]. Properties such as large surface areas, a highly porous structure, and easy functionalization can be counted among the important features of MOFs that deserve this attention[7–9]. They have many cutting-edge applications like storing gas, catalyzing processes, delivering drugs, encapsulating material, supercapacitors, and heavy metal absorbents[10–13].

Compared to other classes of porous materials, MOFs exhibit greater durability, diverse morphologies, and different porosity. MOFs among the porous compounds are stable under various conditions and can maintain porosity due to their chemical and thermal resilience[14–17]. Due to the wide applications of MOF in science and technology, it is of great interest to create new molecular scaffolds with different structures to improve their capacity and selectivity[18–23]. Although MOFs have great potential as heterogeneous catalysts and have attracted great interest from researchers, plans to use them at the industrial stage have yet to make significant progress[13,24,25]. Confinement of the active species within the pores can provide the catalyst with some degree of protection from other reactive species that is difficult to achieve in homogeneous phases through ligand manipulation alone[26,27].

Post-synthetic modification (PSM) through inserting various organic and inorganic functionalities into the framework plays a significant role in optimizing the chemical and physical properties of organic supports such as magnetic nanoparticles, silicates, boehmite, and MOFs[2,13,28–36]. A large variety of supported nanostructured catalysts based on MOFs have been reported during the past decade, highlighting the critical role of such materials in developing novel catalytic materials with high selectivity[37]. One of the most important challenges in catalytic processes is investigating the applications of post-synthetic MOF processes and the formation of organometallic complexes for use in organic synthesis[38].

Thiourea derivatives play a vital role in catalyst modification and synthesis of intermediates and natural products[39,40]. Based on this importance, studies involving new catalyst systems and methodologies continue attracting attention. Different methods for the preparation of thiourea derivatives have been developed. In 2014, Nguyen and colleagues investigated the synthesis of thiourea derivatives from the reaction of isocyanides with aliphatic amines in the presence of elemental sulfur. In another report, a condensation between amines and

Department of Organic Chemistry, Faculty of Chemistry, Bu-Ali Sina University, Hamadan 6517838683, Iran. ✉email: rgvaghei@yahoo.com

carbon disulfide in an aqueous medium allows efficient synthesis of symmetrical and unsymmetrical substituted thiourea derivatives. The synthesis of thiocarbonyl from the combination of sulfur and chloroform in a two-step process was reported by Tan in 2017. A dichloromethane-mediated reaction of carbamoyl isothiocyanates with amines was reported by Linton (SI, Fig. 1, Eqs. 1–4)[41–44]. Most of the hitherto known methods suffer from limitations such as harsh reaction conditions, and use of expensive, toxic catalysts, the formation of side products, and poor yields of desired products. Regarding the important biological properties of synthetic thiourea compounds, an effective procedure for fabricating thiourea derivatives was developed through nitroarene reduction using functionalized MOF (SI, Fig. 1, Eq. 5).

Because nitrobenzenes are toxic, they have adverse effects on humans and other organisms and are a pollutant in the environment[45]. Therefore, developing new catalytic systems for effective and economical removal methods is of great importance. Besides, reducing nitrobenzenes to synthesize thiourea derivatives is a quietly significant synthon in organic synthesis and is present in various pesticides, pharmaceuticals, and fine chemicals[46–48]. Despite developing heterogeneous catalysts with metals such as Pd, Au, Pt, and Mo, selective reduction of nitro compounds is still challenging under mild conditions[47].

Regarding the mentioned points, the present article introduces the design and characterization of a new Cr-based MOF functionalized triazine-aminopyridine via post-synthetic modifications. Triazine-aminopyridine is a recognized and excellent chelating ligand, and we exploited it to anchor Ni ions at the outer shell of MIL-101(Cr)-NH$_2$. Ni NPs species were then successfully decorated on prepared support (MIL-101(Cr)-NH-TA-AP) (Fig. 1). The catalytic activities of this successfully synthesized nanocatalyst were tested in synthesizing thiourea derivatives through nitrobenzene reduction. Operational simplicity, green reaction conditions, simple and inexpensive procedure, high efficiency, short reaction times, easy catalyst separation, and reusability for several consecutive cycles are the key advantages of this protocol. The other key advantage of this protocol is that the reactions were found to be complete at room temperature. This method is found to tolerate substrates having electron-donating and withdrawing functionalities. In addition to the above advantages, we also observed this transformation is equally effective in water as a green solvent.

Experimental

Synthesis of MIL101 (Cr)-NH$_2$.   MIL101 (Cr)-NH$_2$ was synthesized using solvothermal methods[49].

Synthesis of triazine-aminopyridine-modified MIL-101(Cr)-NH$_2$ MOF (MIL-101(Cr)-NH-TA-AP).   A solution of cyanuric chloride (0.75 g; 4 mmol), MIL-101(Cr)-NH$_2$ (0.5 g), and DMF (10 mL) was stirred at ambient temperature for 12 h. In the next step, 2-aminopyridine (0.94 g; 8 mmol) was added and stirred for 12 h. The obtained residue was filtered and washed with ethanol (2×10 mL) and dried in a vacuum desiccator to obtain MIL-101(Cr)-NH-TA-AP as a stable powder.

Synthesis of MIL-101(Cr)-NH-TA-AP/Ni nanocomposite.   Nickel nanoparticles were immobilized on the surface of the synthesized MIL-101(Cr)-NH-TA-AP according to the previous methods (Fig. 1).

General method for the fabrication of thiourea derivatives.   A mixture of nitrobenzene analogs (1 mmol), sodium borohydride (1.5 mmol), phenyl isocyanate (1 mmol), and MIL-101(Cr)-NH-TA-AP/Ni (50 mg, 0.1 mol%) was stirred at room temperature in H$_2$O (2 mL) for the suitable time, as illustrated in Table 2. After the end of the reaction, the catalyst was filtered off. The residue was extracted with ethyl acetate to obtain pure products in 91–98% yields.

Results and discussion

Figure 2 illustrates the FT-IR absorption spectra of MIL-101(Cr)-NH$_2$, MIL-101(Cr)-NH-TA-AP, and MIL-101(Cr)-NH-TA-AP/Ni. The stretching vibrations at 3400 cm^{-1} indicate the symmetric modes of the N–H bonds attached to the Cr atoms (Fig. 2a)[50]. Comparing spectra of MIL-101(Cr)-NH-TA-AP and MIL-101(Cr)-NH-TA-AP/Ni (Fig. 2b,c with Fig. 2a) confirmed the successful functionalization. Finally, considering the MIL-101(Cr)-NH-TA-AP/Ni catalyst spectra, the C=N vibration shifts around 1663 cm^{-1} due to the interaction between MIL-101(Cr)-NH-TA-AP and Ni NPs (1685 vs. 1663 cm^{-1}). Moreover, the bending vibration of NH$_2$ in the MIL-101(Cr)-NH-TA-AP/Ni shifts around 3338 cm^{-1} (3422 vs. 3338 cm^{-1}).
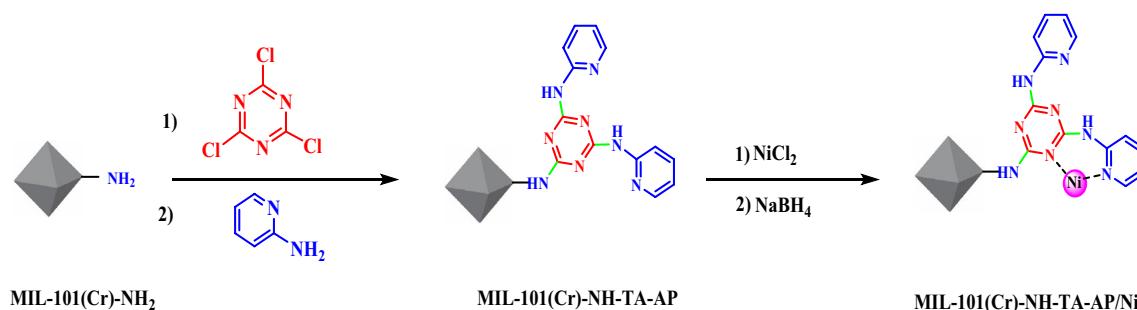

**Figure 1.** Preparation of MIL-101(Cr)-NH-TA-AP/Ni nanocatalyst.
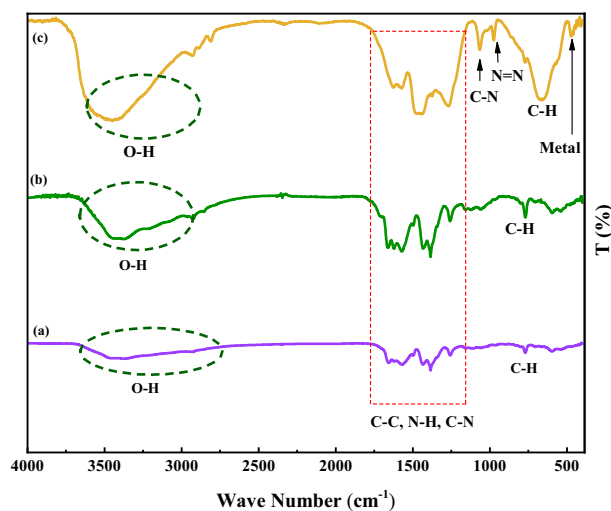
Figure 2. FT-IR spectra of (**a**) MIL-101(Cr)-NH$_2$, (**b**) MIL-101(Cr)-NH-TA-AP, and (**c**) MIL-101(Cr)-NH-TA-AP/Ni.

XRD analysis was used to check the crystal structure of MIL-101(Cr)-NH$_2$ and MIL-101(Cr)-NH-TA-AP/Ni samples (Fig. 3). The major diffraction peaks of MIL-101(Cr)-NH$_2$ appeared at 2θ angles of 3.25°, 8.41°, 9.02°, 10.5°, and 16.49°, which are in agreement with pattern reported in the literature (Fig. 3a)[49,50]. In the XRD spectrum of MIL-101(Cr)-NH-TA-AP/Ni, a minor shift in position and width, few intense peaks, and several sharp peaks in the pattern are observed, confirming the successful formation of the mentioned nanocatalyst (Fig. 3b). Moreover, the presence of sharp peaks in 2θ between 10° and 50° suggests the successful functionalization of MIL-101(Cr)-NH$_2$. Afterward, using Scherrer and Bragg's equations, the average monthly distance and crystal size was determined to be 40 nm. These results are in good agreement with the result obtained from SEM images. Figure 3c illustrates XRD patterns of recycled MIL-101(Cr)-NH-TA-AP/Ni nanocomposite. As clearly can be seen from the XRD image, the catalyst retains its initial crystallinity and particles size (Fig. 3c). Since post-synthetic modification of MIL-101(Cr)-NH$_2$ leads to the synthesis of the final catalyst with less crystallinity, and the simulated pattern is only used for single crystal materials, in this research, the simulated pattern of MIL-101(Cr)-NH$_2$ was added to Fig. 3. In the functionalized MOF, due to the presence of functional groups, the triazine-aminopyridine groups occupy the available surface of the MOF. As a result, some peaks are removed, which is consistent with previous studies[51].

SEM analysis was applied to examine the morphological and chemical changes of MIL-101(Cr)-NH-TA-AP/Ni. The SEM image of the MIL-101(Cr)-NH indicates almost a spherical structure morphology. In addition, according to Fig. 4A–D, there is no significant change even after the immobilization of metal species. It is of note that functionalized MOF can retain Ni NPs species in the pores and prevent their agglomeration (Fig. 4E–H).
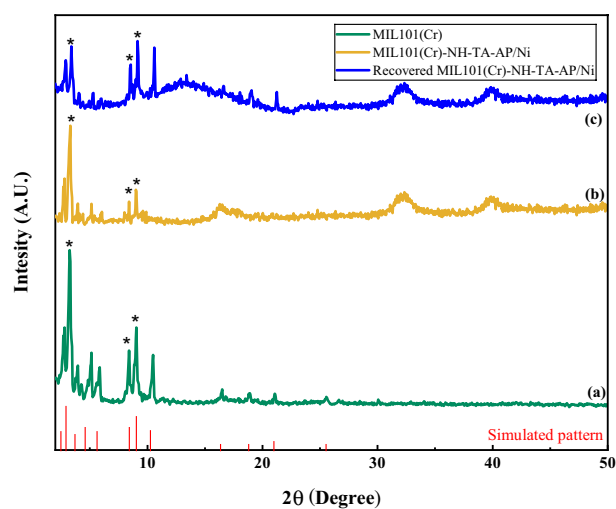
**Figure 3.** XRD pattern of MIL-101(Cr) (**a**), MIL-101(Cr)-NH-TA-AP/Ni (**b**), and recovered MIL-101(Cr)-NH-TA-AP/Ni (**c**).
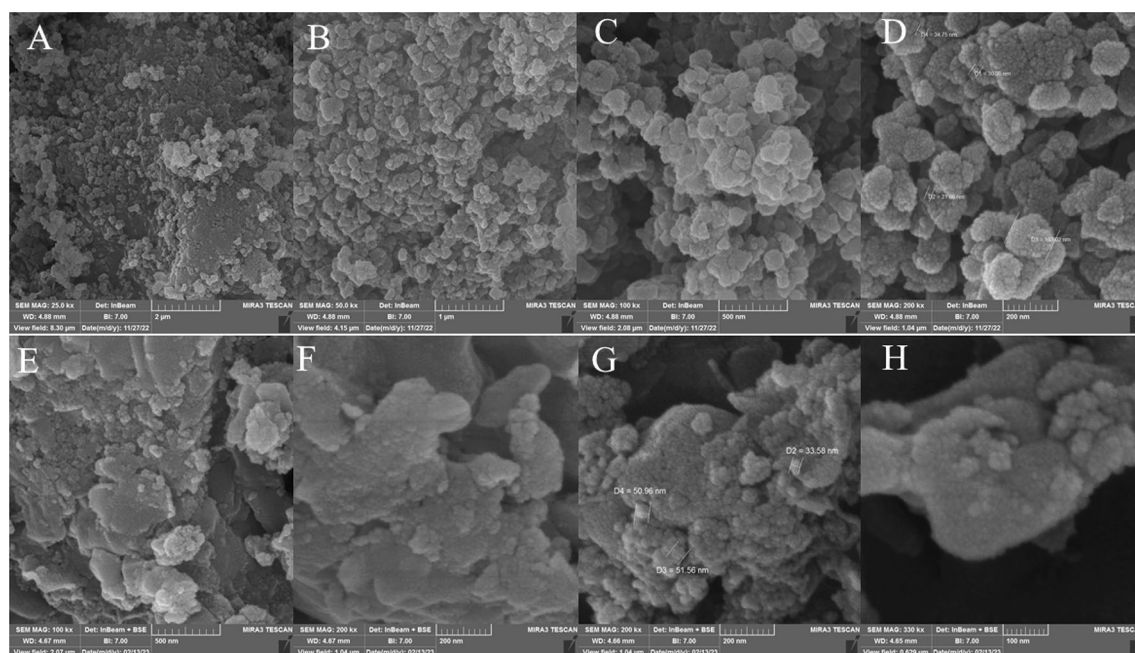
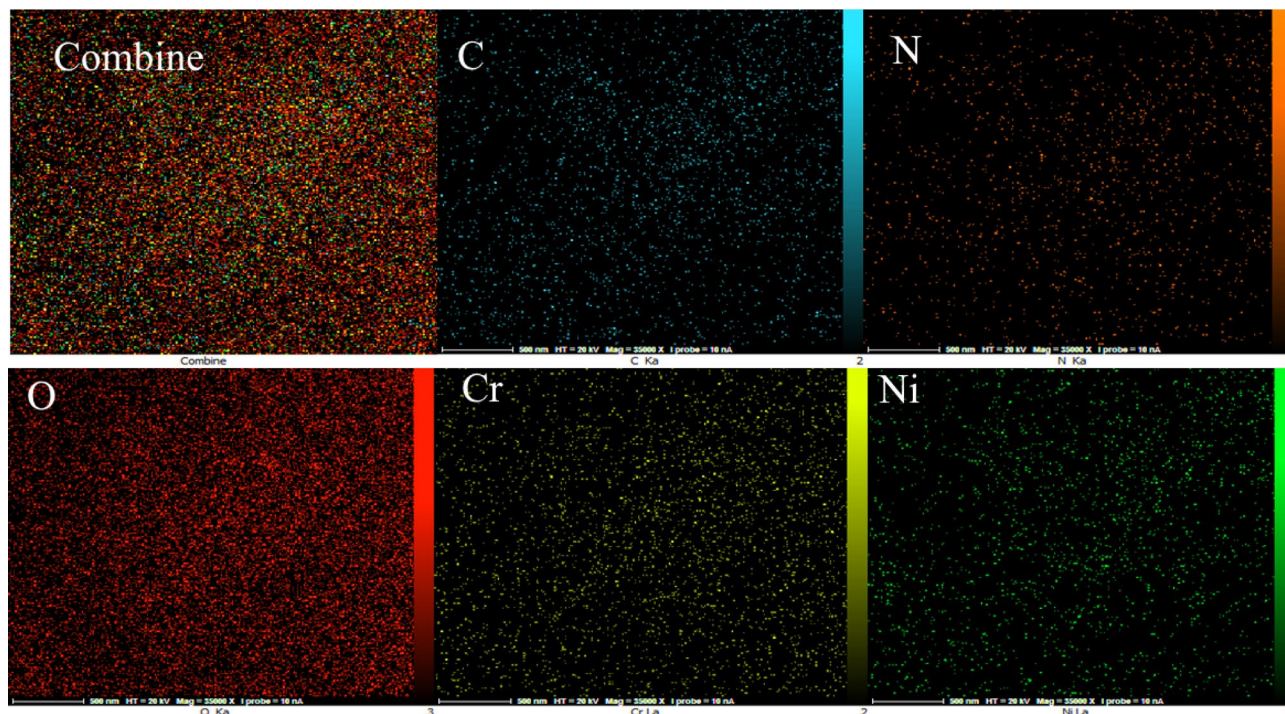**Figure 4.** FESEM images of MIL-101(Cr)-NH$_2$ (**A–D**) and MIL-101(Cr)-NH-TA-AP/Ni (**E–H**).

The elemental analysis of the present MIL-101(Cr)-NH-TA-AP/Ni catalyst is presented in Fig. 5. The elemental mapping of MIL-101(Cr)-NH-TA-AP/Ni nanocatalyst is depicted in Fig. 6. As can be seen, Cr, N, C, Ni, and O elements are present in the structure of nanocatalyst with a uniform distribution.

Nitrogen adsorption–desorption isotherm measurement of MIL-101(Cr)-NH-TA-AP was undertaken to confirm the porous nature of the catalyst and estimate their surface area (Fig. 7a). The analysis of the BET revealed the formation of nanoparticles with a total pore volume of 0.15 cm^3/g, an average pore diameter of 10.61 nm, and a surface area of 22.04 m^2/g (Table 1). The adsorption isotherm is type IV, and the presence of mesoporous structure in the material is evident from the appearance of the hysteresis loop. From this BET analysis, it is inferred that our nano-support has a mesoporous nature surface and huge surface area, which is a primary property of excellent catalysts. Figure 7b shows the N$_2$ adsorption and desorption isotherms of the MIL-101(Cr)-NH-TA-AP/Ni. These isotherms exhibit type V isotherms (typical of mesopores) and type H3 hysteresis loops (indicating slit-shaped pores). According to the Langmuir adsorption isotherm, the specific surface area of the MIL-101(Cr)-NH-TA-AP/Ni is 17.16 m^{2}g^{-1}. Figure 7c presents the N$_2$ adsorption and desorption isotherms of the recovered MIL-101(Cr)-NH-TA-AP/Ni. They indicate type V isotherms (typical of mesopores) and type H3 hysteresis loops (indicating slit-shaped pores). According to the Langmuir adsorption isotherm, the specific surface area of the recovered MIL-101(Cr)-NH-TA-AP/Ni is 7.36 m^{2}g^{-1}. The changes associated with the textural properties of the 6th reused catalyst can be due to the distribution of the reactants inside the pores (Table 1).

Figure 8 shows the TGA curves showing the residual masses of MIL-101(Cr)-NH-TA-AP/Ni in the temperature range of 25 to 600 °C. The TGA curve initially displays an imperceptible weight loss of 17% in the region

Elements	Weight%	Atomic%
C	11.91	16.31
N	7.44	8.73
O	69.62	71.56
Cr	8.73	2.76
Ni	2.30	0.65
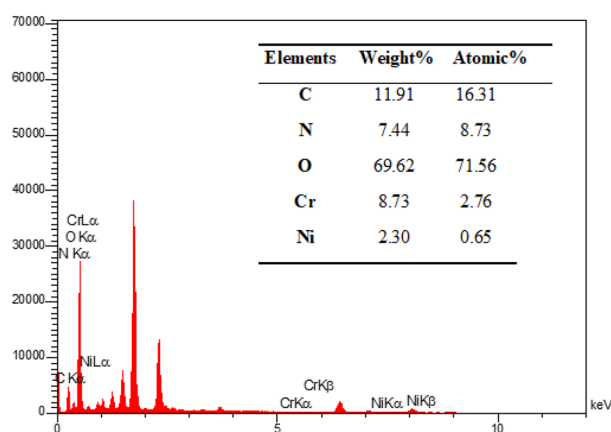
**Figure 5.** EDX spectrum of MIL-101(Cr)-NH-TA-AP/Ni.

Figure 6. Elemental mapping of MIL-101(Cr)-NH-TA-AP/Ni.

90–180 °C, which verifies the loss of solvent absorbed at the surface of MIL-101(Cr)-NH-TA-AP/Ni [52]. A significant weight loss of 35% in the 200–600 °C range can be explained by the decomposition of the immobilized ligand on the surface of MIL-101(Cr)-NH$_2$. Thermal characterization data for MIL-101(Cr)-NH-TA-AP/Ni display that the catalyst was stable up to 220 °C. With increasing temperature up to 450 °C, due to the decomposition of the framework, a considerable decrease occurred in the thermal stability of MIL-101(Cr)-NH-TA-AP/Ni (Fig. 8a). The thermal and behavioral stability of the recovered MIL-101(Cr)-NH-TA-AP/Ni were studied by thermal gravimetric (TG) technique. TGA of the recovered catalyst after the 6th recycle run is also stable over a wide temperature range of 25–600 °C (Fig. 8b).

Optimization conditions. The optimum conditions were selected by studying the effect of solvent on the reaction rate for the preparation of 1,3-diphenyl thiourea by condensation of nitrobenzene and phenyl isocyanate in the presence of 0.1 mol% (MIL-101(Cr)-NH-TA-AP/Ni) under different solvents (e.g., ethanol, methanol, EtOH:H$_2$O, toluene, and H$_2$O) at 50℃ (Table 2, entry 1–5). Overall, the best results were obtained with 0.1 mol% MIL-101(Cr)-NH-TA-AP/Ni using water solvent (Table 2, entry 5). Moreover, the study set of experiments determines the optimal amount of catalyst MIL-101(Cr)-NH-TA-AP/Ni require for the reaction. The reaction was carried out by variable amounts of catalyst (Table 2, entries 6–7), and maximum yield was found with 0.1 mol% of the catalyst. Further increasing the amount of catalyst MIL-101(Cr)-NH-TA-AP/Ni in the mentioned reaction condition did not significantly improve product yields (Table 2, entry 7). Examining the model reaction at room temperature demonstrated that temperature is essential to the reaction efficiency (Table 2, entry 8). The response of the studied model at different times showed that the highest yield and conversion were obtained at 30 min (Table 2, entry 9). Finally, the efficacy of the catalyst was evaluated by performing the sample reaction by MIL-101(Cr)-NH$_2$-Ni. The results indicate the functionalized MOF provides the required product with great efficiency (Table 2, entry 10 vs. 5).

The generality of the method was demonstrated using different substituted nitrobenzenes. The reaction scope was expanded, and excellent reaction conversions were obtained with nitrobenzenes having electron-donating and electron-withdrawing groups. This finding reveals that the substituents on nitrobenzene have no noticeable effect on the reaction conversion (Table 3). In this work, new thiourea derivatives were developed innovatively (entries 2, 5, 8, and 9).

The proposed synthesis mechanism for phenyl thiourea is illustrated in Fig. 9. The mesoporous nature of MIL-101(Cr)-NH-TA-AP/Ni catalyst gives it unique characteristics like high surface area, tunable pore size, and large pore volume, which favor their enhanced accessibility to active sites with improved mass transport/ diffusion. A hydride molecule is transferred to the nitro group by adsorbing sodium borohydride on the NPs' surface. The nitroso intermediate **A**, formed by water elimination, adsorbed on the MIL-101(Cr)-NH-TA-AP/Ni, is again reduced by the hydride transfer from sodium borohydride to the hydroxylamine B. This intermediate is
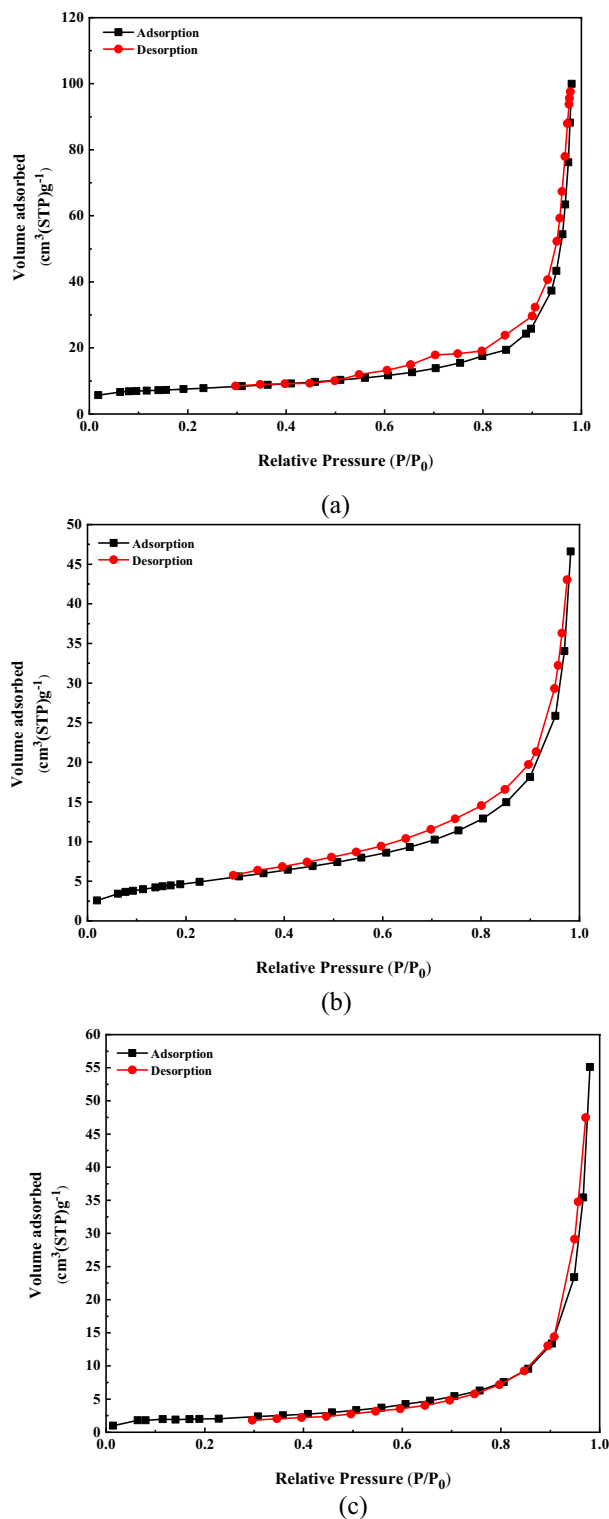
Figure 7. N_2 adsorption isotherms by the BET analysis of MIL-101(Cr)-NH-TA-AP (**a**), MIL-101(Cr)-NH-TA-AP/Ni (**b**), and Recovered MIL-101(Cr)-NH-TA-AP/Ni (**c**).

Parameter	MIL-101(Cr)-NH-TA-AP	MIL-101(Cr)-NH-TA-AP/Ni	Recovered MIL-101(Cr)-NH-TA-AP/Ni
a_s (m^2/g)	32.97	17.16	7.36
V_m (cm^3(STP) g^{-1})	7.57	3.95	1.69
V_p (cm^{3}g^{-1})	0.15	0.072	0.085
r_p (nm)	10.61	1.63	12.24
a_p (m^2/g)	22.04	18.73	10.83

Table 1. Results of the Langmuir and BET measurements of MIL-101(Cr)-NH-TA-AP, MIL-101(Cr)-NH-TA-AP/Ni, and Recovered MIL-101(Cr)-NH-TA-AP/Ni.
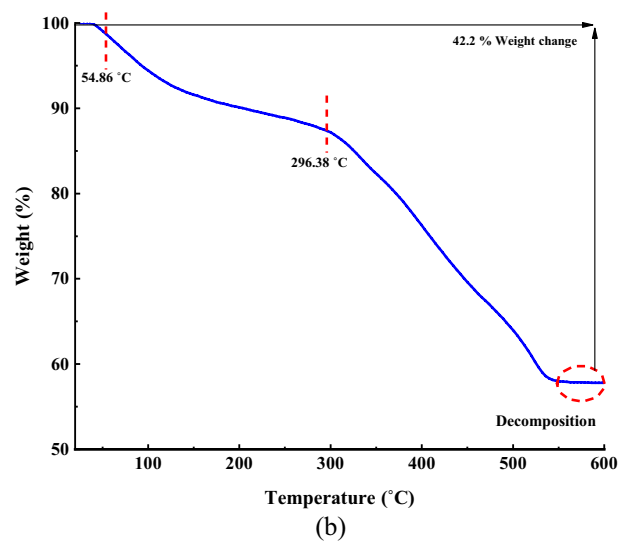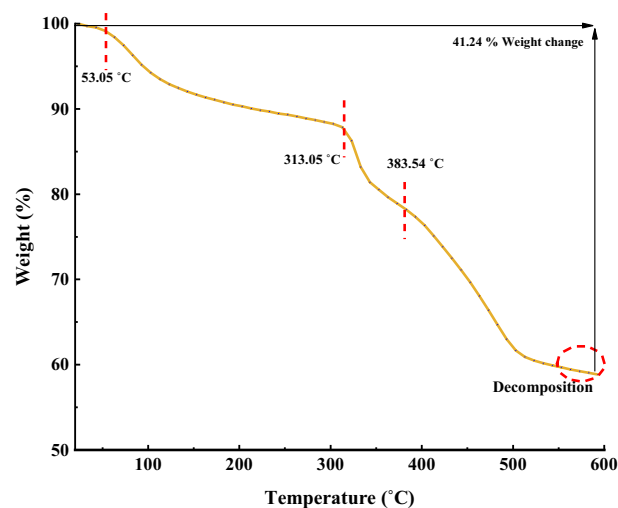
Figure 8. TGA curve of (**a**) MIL-101(Cr)-NH-TA-AP/Ni and (**b**) MIL-101(Cr)-NH-TA-AP/Ni after recycling.

Entry	T (°C)	Cat (mol%)	Solvent	Time (min.)	Yield (%)[a]	TOF(h^{-1})
1	50	0.10	Toluene	30	48	120
2	50	0.10	Methanol	30	60	600
3	50	0.10	EtOH	30	70	700
4	50	0.10	EtOH/H_2O	30	80	800
5	50	0.10	H_2O	30	98	**980**
6	50	0.05	H_2O	30	67	1340
7	50	0.12	H_2O	30	98	816.6
8	r.t	0.10	H_2O	30	70	700
9	50	0.10	H_2O	15	51	2000
10	50	50 mg	H_2O	30	58	580[b]

Table 2. Optimization of the reaction conditions using MIL-101(Cr)-NH-TA-AP/Ni. [a]Reaction conditions: nitrobenzene (1.0 mmol), MIL-101(Cr)-NH-TA-AP/Ni, sodium borohydride (1.5 mmol), and H_2O (2 mL).[b] The model reaction was investigated in the presence of MIL-101(Cr)-NH$_2$-Ni.
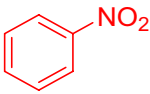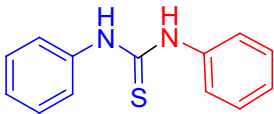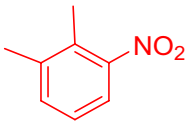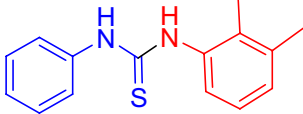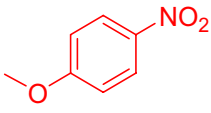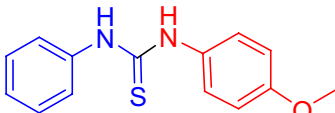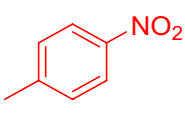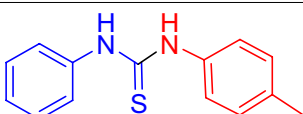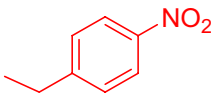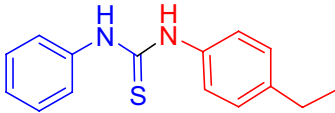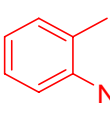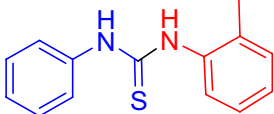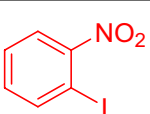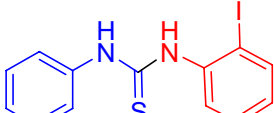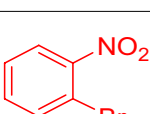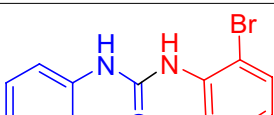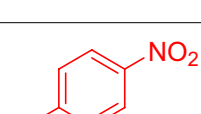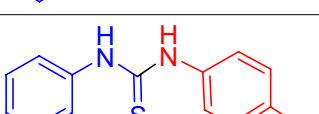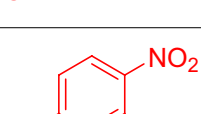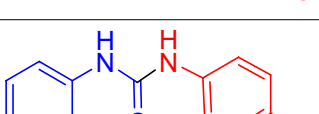
further reduced to the aniline[60,61]. Lastly, phenylthiourea is obtained by the reaction between aniline and phenyl isocyanate.

The robustness of the MIL-101(Cr)-NH-TA-AP/Ni nanocomposite, as an imperative distinctiveness of catalyst in practical applications of organic transformation, was examined by successive six runs (i.e., 98, 96, 95, 93, 91, and 88). The MIL-101(Cr)-NH-TA-AP/Ni solid was recycled via simple filtration and washed with ethanol. The catalyst MIL-101(Cr)-NH-TA-AP/Ni reusability was checked in the synthesis of 1,3-diphenyl thiourea. Based on the obtained results, robust and excellent chemical stability of MIL-101(Cr)-NH-TA-AP/Ni is confirmed by FESEM, FTIR, and EDX-elemental mapping spectral analysis after six runs (Fig. 10). The FTIR of recycled catalyst confirme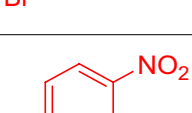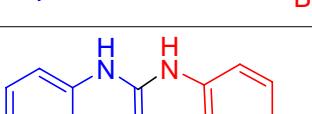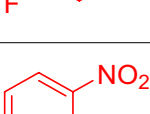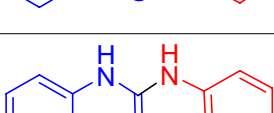d the stability of the catalysts as the regeneration data do not exhibit any change after the initial patterns (Fig. 10a). In addition, FESEM of the catalyst after the 6th recycling (Fig. 10b) along with EDX-elemental mapping spectra (Fig. 10c,d) demonstrates the presence of Ni and functionalized MIL-101(Cr)-NH$_2$ on the catalyst surface. The results show that the catalyst retains its initial morphology and structure without any change. As can be seen from EDX data and elemental mapping, no change occurs in elemental composition, validating the robustness of our material. The histogram in Fig. 11 represents the recyclability of the fabricated nanocatalyst for the synthesis of 1,3-diphenyl thiourea. The minor reduction observed in the catalytic ability is likely due to the normal dissipation of the catalyst in the workup process. Here, nickel concentration determined by ICP analysis changed from 8.79 mmol/g to 8.76 mmol/g after the 6th run. Therefore, the MIL-101(Cr)-NH-TA-AP/ Ni nanocomposite is highly stable under the studied reaction conditions.

Conclusion

We introduced a triazine-aminopyridine-modified MIL-101(Cr)-NH$_2$ metal–organic framework (MOF) with Ni NPs decorated over its surface. Ni NPs were immobilized following a post-functionalization of triazine-aminopyridine over the core MIL-101(Cr)-NH$_2$ MOF than the typical surface deposition. The excellent chelating potential of triazine-aminopyridine was exploited to deposit Ni NPs over it. The material's structural morphology and physicochemical features were explored over different instrumental methods. In addition, atomic mapping analysis displays the uniform dispersion of active sites throughout the surface matrix. The nanocatalyst was used to synthesize thiourea derivatives through nitrobenzene reduction under mild and green conditions affording outstanding yields. The material's robustness was validated by recycling it for 6 consecutive cycles without considerable loss of its reactivity. Moreover, Ni species had negligible leaching in the reaction medium, justifying its true heterogeneity.

Entry	Substrate	Product	Time (min)	Yield (%)[a]	Melting point	References
1			30	98	140–142	152[53]
2			35	97	138–140	–
3			30	99	152–154	159–161[54]
4			30	96	135–136	138–139 [55]
5			35	92	127–129	–
6			30	97	138–139	138[56]
7			35	95	160–162	160[57]
8			40	96	156–157	–
9			40	93	152–154	–
10			40	91	160–162	158[58]
11			25	92	173–176	171–172[59]
12			20	94	172–175	172–174[59]

Table 3. Synthesis of thiourea derivatives from nitrobenzenes. Reaction conditions: nitrobenzene (1.0 mmol), MIL-101(Cr)-NH-TA-AP/Ni (0.1 mol%), sodium borohydride (1.5 mmol), and H_2O (2 mL). [b]Isolated yield.
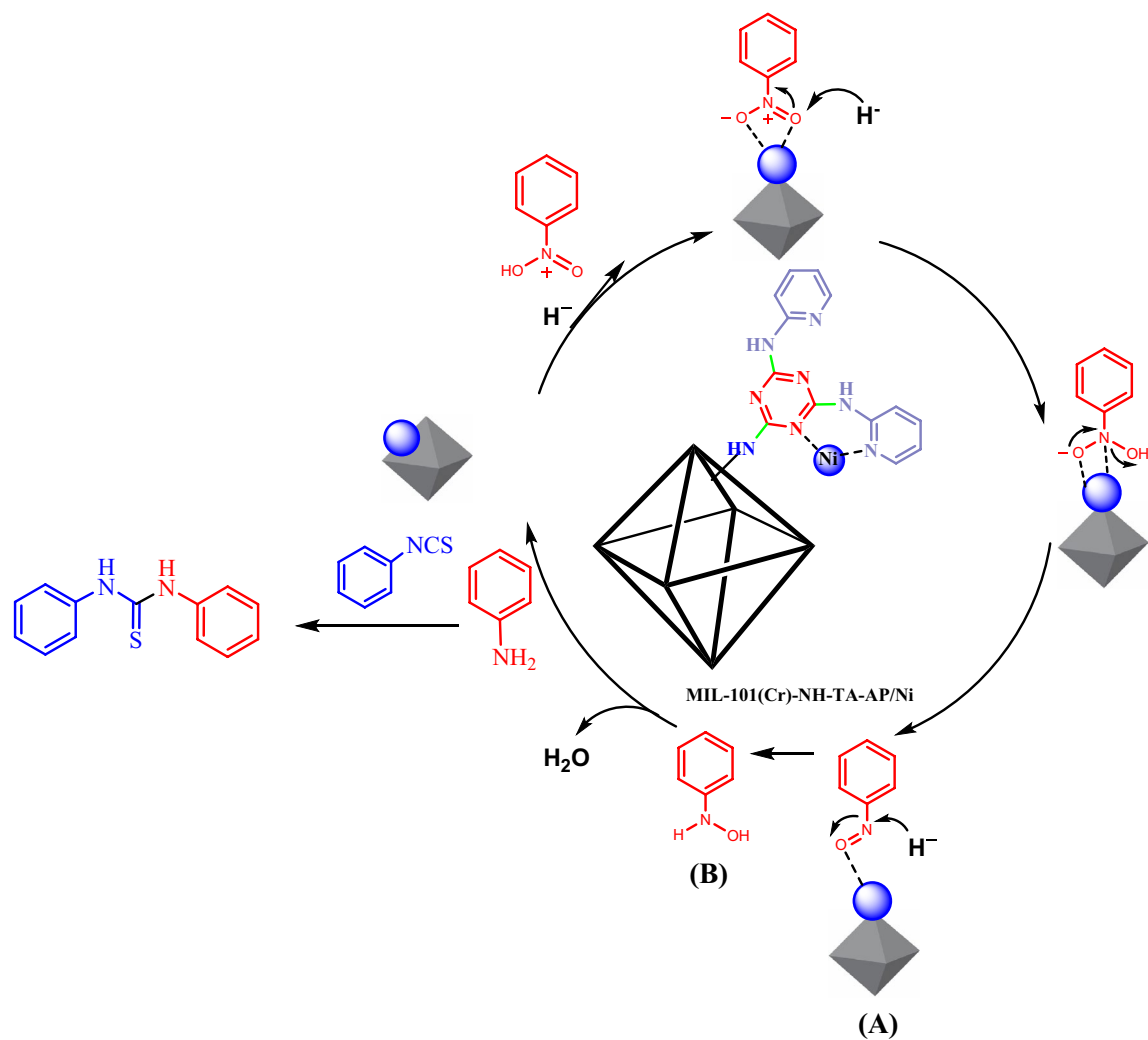
Figure 9. The mechanistic pathway proposed for the synthesis of thiourea from nitrobenzene derivatives.
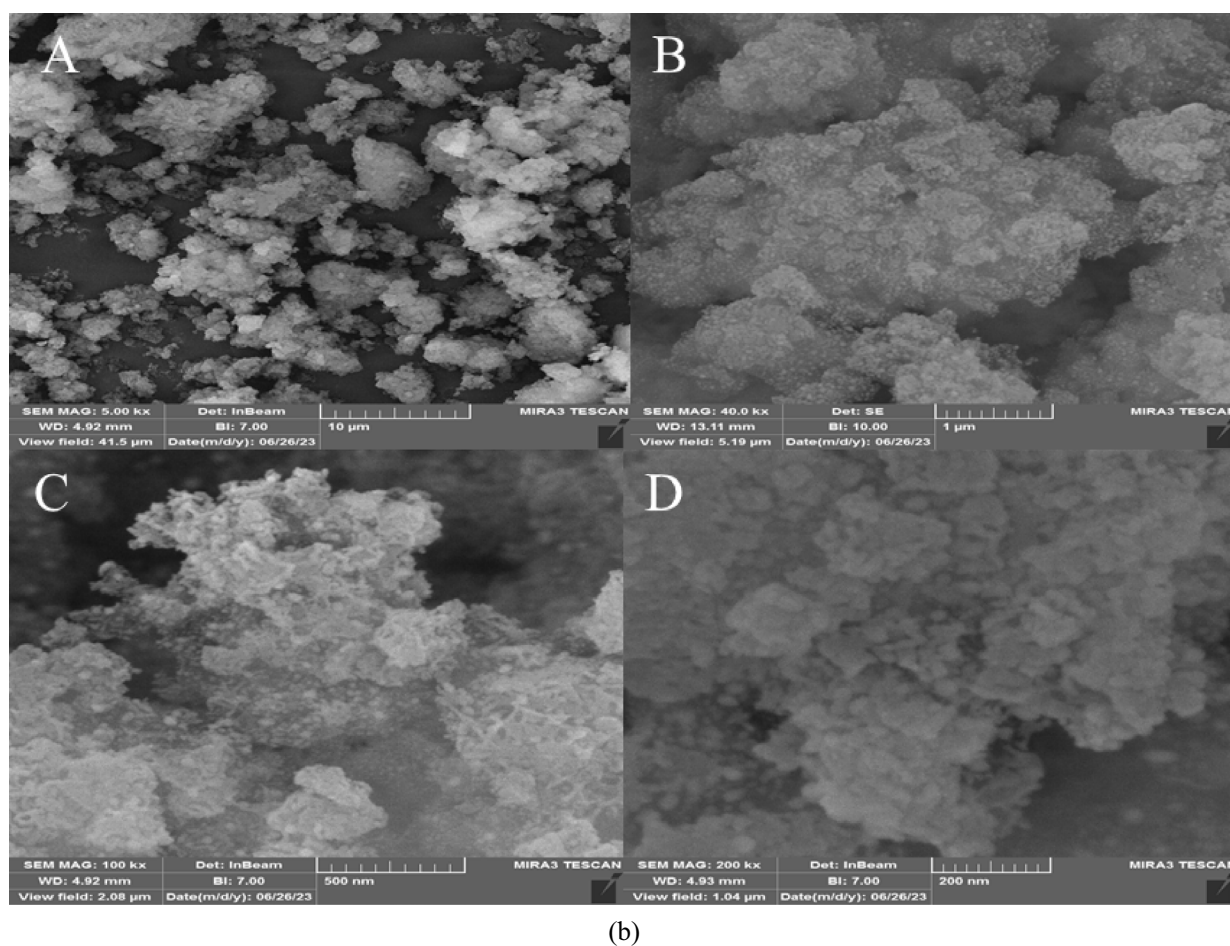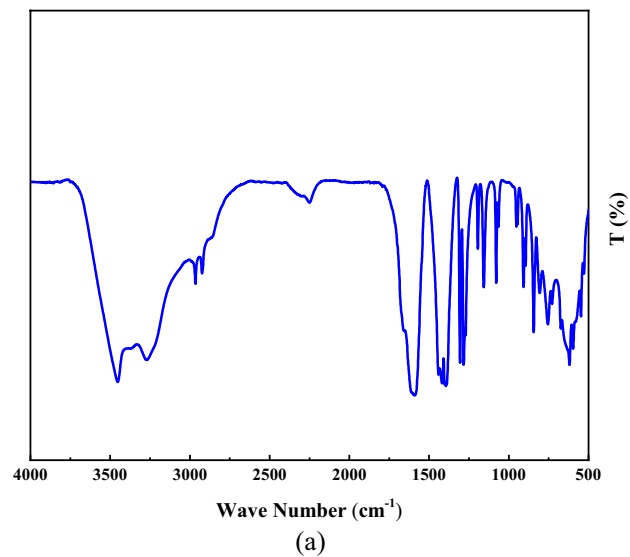
Figure 10. FTIR (**a**), FESEM (**b**), EDX (**c**), and elemental mapping analysis of recycled catalyst (**d**) after six runs.
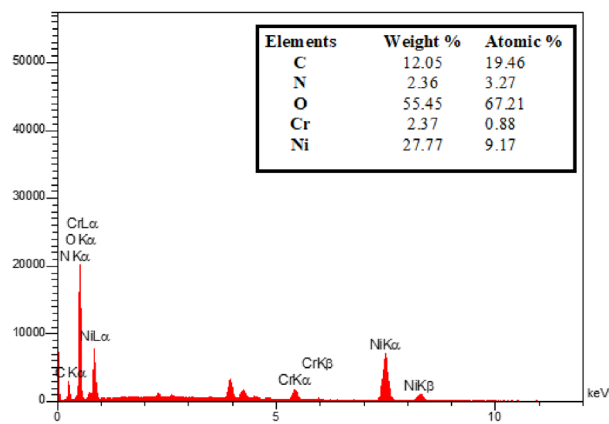
(c)
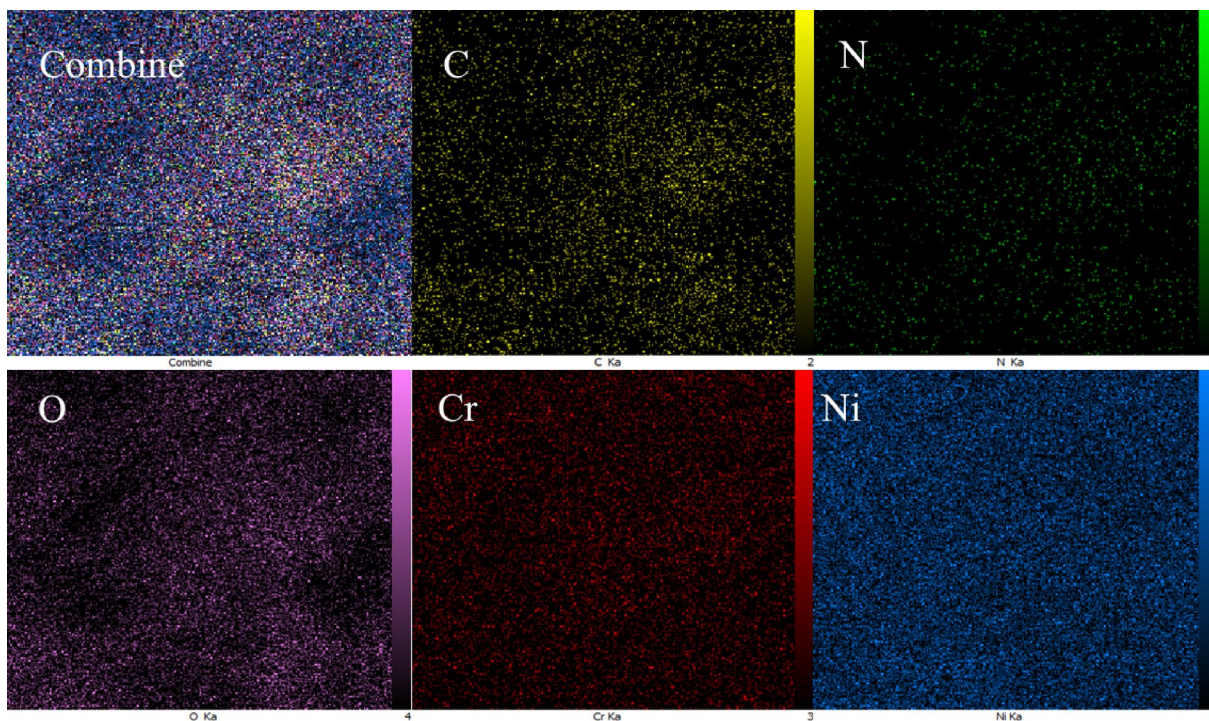
(d)

Figure 10. (continued)
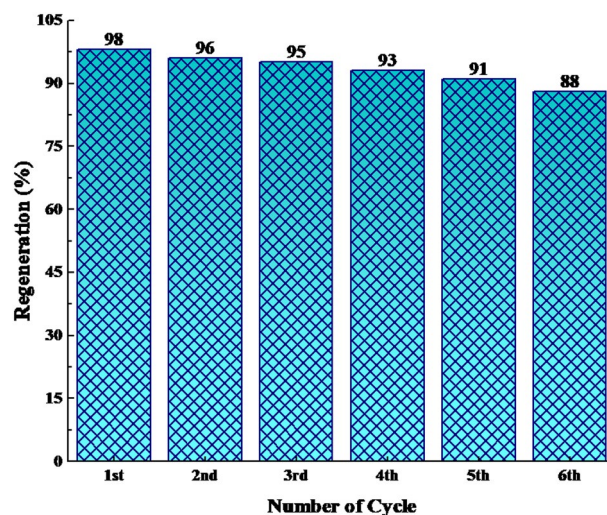
Figure 11. Reusability of the synthesized catalyst in the condensation of nitrobenzene and phenyl isocyanate.

Data availability

All data generated or analyzed during this study are included in this published article [and the supplementary information file].

References

1. Zhang, C.-L. *et al.* Microenvironment modulation of metal-organic frameworks (MOFs) for coordination olefin oligomerization and (co)polymerization. *Small* https://doi.org/10.1002/smll.202205898 (2022).
2. Dhakshinamoorthy, A., Asiri, A. M. & García, H. Metal-organic frameworks as multifunctional solid catalysts. *Trends Chem.* **2**, 454–466 (2020).
3. Ramish, S. M., Ghorbani-Choghamarani, A. & Mohammadi, M. Microporous hierarchically Zn-MOF as an efficient catalyst for the Hantzsch synthesis of polyhydroquinolines. *Sci. Rep.* **12**, 1479 (2022).
4. Altass, H. M. *et al.* Exploitation the unique acidity of novel cerium-tungstate catalysts in the preparation of indole derivatives under eco-friendly acid catalyzed Fischer indole reaction protocol. *Arab. J. Chem.* **15**, 103670 (2022).
5. Alasri, T. M. *et al.* Band-structure engineering of TiO$_2$ photocatalyst by AuSe quantum dots for efficient degradation of malachite green and phenol. *J. Inorg. Organom. Polym.* **33**, 1729–1740 (2023).
6. Altass, H. M. *et al.* Highly efficient, recyclable cerium-phosphate solid acid catalysts for the synthesis of tetrahydrocarbazole derivatives by Borsche-Drechsel cyclization. *Reac. Kinet. Mech. Cat.* **134**, 143–161 (2021).
7. Wang, Z. *et al.* Recent advances in porphyrin-based MOFs for cancer therapy and diagnosis therapy. *Coord. Chem. Rev.* **439**, 213945 (2021).
8. Tajahmadi, S. *et al.* Metal-organic frameworks: A promising option for the diagnosis and treatment of Alzheimer's disease. *J. Control. Release* **353**, 1–29 (2023).
9. Ghorbani-Choghamarani, A., Taherinia, Z. & Mohammadi, M. Facile synthesis of Fe$_3$O$_4$@GlcA@Ni-MOF composites as environmentally green catalyst in organic reactions. *Environ. Technol. Innov.* **24**, 102050 (2021).
10. Rasheed, T. *et al.* Environmental threatening concern and efficient removal of pharmaceutically active compounds using metal-organic frameworks as adsorbents. *Environ. Res.* **185**, 109436 (2020).
11. Sharafinia, S., Farrokhnia, A. & Ghasemian Lemraski, E. The adsorption of cationic dye onto ACPMG@ZIF-8 core-shell, optimization using central composite response surface methodology (CCRSM). *Colloids Surf. A: Physicochem. Eng.* **634**, 128039 (2022).
12. Sharafinia, S., Farrokhnia, A., Lemraski, E. G. & Rashidi, A. Decoration of ZnFe$_2$O$_4$ and UiO-66 over g-C3N4 as magnetically novel reusable visible light photocatalyst for degradation of Rh–B. *Opt. Mater.* **132**, 112838 (2022).
13. Keypour, H. *et al.* Post-synthetic modification of dual-porous UMCM-1-NH2 with palladacycle complex as an effective heterogeneous catalyst in Suzuki and Heck coupling reactions. *J. Organom. Chem.* **989**, 122646 (2023).
14. Yilmaz, B., Trukhan, N. & Müller, U. Industrial outlook on zeolites and metal organic frameworks. *Cuihua Xuebao/Chin. J. Catal.* **33**, 3–10 (2012).
15. Koolivand, M. *et al.* A novel cubic Zn-citric acid-based MOF as a highly efficient and reusable catalyst for the synthesis of pyrano-pyrazoles and 5-substituted 1H-tetrazoles. *Appl. Organom. Chem.* **36**, 2641–2663 (2022).
16. Li, Y. & Wen, G. Advances in metal-organic frameworks for acetylene storage. *Eur. J. Inorg. Chem.* **2020**, 2303–2311 (2020).
17. Naghdi, S. *et al.* Recent advances in application of metal-organic frameworks (MOFs) as adsorbent and catalyst in removal of persistent organic pollutants (POPs). *J. Hazard. Mater.* **442**, 130127 (2023).
18. Wang, G., Wang, J., Chen, Z. & Hu, J. Metal-organic framework grown in situ on chitosan microspheres as robust host of palladium for heterogeneous catalysis: Suzuki reaction and the p-nitrophenol reduction. *Int. J. Biol. Macromol.* **206**, 232–241 (2022).
19. Nguyen, L. H. T. *et al.* Fe-based metal-organic framework as a chemo resistive sensor for low-temperature monitoring of acetone gas. *Sens. Actuators B* **388**, 133799 (2023).
20. Matheu, R. *et al.* Postsynthetic metalation of a new metal–organic framework to improve methane working storage capacity. *ACS Mater. Lett.* **11**, 2375–2380 (2022).
21. Yang, D. H. *et al.* Novel amine-functionalized zinc-based metal-organic framework for low-temperature chemo resistive hydrogen sensing. *Sens. Actuators B* **368**, 13212 (2022).
22. Dang, M. H. D. *et al.* Using sulfate-functionalized Hf-based metal–organic frameworks as a heterogeneous catalyst for solvent-free synthesis of pyrimido[1,2-a] benzimidazoles *via* one-pot three-component reaction. *J. Ind. Eng. Chem.* **103**, 340–347 (2021).

23. Dang, M.-H.D. *et al.* An effective combination of reusable Pd@MOF catalyst and deep eutectic solvents for high-performance C-C coupling reaction. *J. Ind. Eng. Chem.* **111**, 111–120 (2022).

24. Wang, T., Cao, X. & Jiao, L. MOFs-derived carbon-based metal catalysts for energy-related electrocatalysis. *Small* **17**, 2004398 (2021).

25. Luo, H., Gu, Y., Liu, D. & Sun, Y. Advances in oxidative desulfurization of fuel oils over mofs-based heterogeneous catalysts. *Catalysts* **11**, 1557 (2021).

26. Zhang, R., Chen, Y., Ding, M. & Zhao, J. Heterogeneous Cu catalyst in organic transformations. *Nano Res.* **15**, 2810–2833 (2022).

27. Lorignon, F., Gossard, A. & Carboni, M. Hierarchically porous monolithic MOFs: An ongoing challenge for industrial-scale effluent treatment. *Chem. Eng. J.* **393**, 124765 (2020).

28. Kazemi, M. & Mohammadi, M. Magnetically recoverable catalysts: Catalysis in synthesis of polyhydroquinolines. *Appl. Organomet. Chem.* **34**, e5400 (2020).

29. Salama, R. S. Synthesis, characterization and catalytic activities of sulfuric acid loaded on copper metal organic frameworks (Cu-BDC). *Delta Univ. Sci. J.* **2**, 10–15 (2019).

30. Altass, H. M. *et al.* Low temperature CO oxidation over highly active gold nanoparticles supported on reduced graphene oxide@ Mg-BTC nanocomposite. *Catal. Lett.* **153**, 876–886 (2023).

31. Alshorifi, F. T., Tobbala, D. E., El-Bahy, S. M., Nassan, M. A. & Salama, R. S. The role of phosphotungstic acid in enhancing the catalytic performance of UiO-66 (Zr) and its applications as an efficient solid acid catalyst for coumarins and dihydropyrimidinones synthesis. *Cat. Com.* **169**, 106479 (2022).

32. Al-Thabaiti, S. A., Mostafa, M. M., Ahmed, A. I. & Salama, R. S. Synthesis of copper/chromium metal organic frameworks-Derivatives as an advanced electrode material for high-performance supercapacitors. *Ceram. Int.* **49**, 5119–5129 (2023).

33. Salama, R. S., *et al. Delta Univ. Sci. J.*, **6**, 266–277 (2023).

34. Gharehkhani, A., Ghorbani-vaghei, R. & Alavinia, S. Synthesis of calixresorcarenes using magnetic poly triazine-benzene sulfonamide-SO$_3$H. *RSC Adv.* **11**, 37514–37527 (2021).

35. Rahimi, A., Ghorbani-Vaghei, R. & Alavinia, S. Nickel nanoparticles anchored over porous triazine-thiourea-sulfonamide to explore the reduction of carbonyl compounds. *J. Porous Mater.* **28**, 1643–1653. https://doi.org/10.1007/s10934-021-01104-1 (2021).

36. Nouri, F., Rostamizadeh, S. & Azad, M. Post-synthetic modification of IRMOF-3 with an iminopalladacycle complex and its application as an effective heterogeneous catalyst in Suzuki-Miyaura cross-coupling reaction in H$_2$O/EtOH media at room temperature. *Mol. Catal.* **443**, 286–293 (2017).

37. Yang, D. & Gates, B. C. Catalysis by metal organic frameworks: Perspective and suggestions for future research. *ACS Catal.* **9**, 1779–1798 (2019).

38. Ghobakhloo, F., Azarifar, D., Mohammadi, M., Keypour, H. & Zeynali, H. Copper(II) schiff-base complex modified UiO-66-NH2(Zr) metal-organic framework catalysts for knoevenagel condensation-michael addition-cyclization reactions. *Inorg. Chem.* **61**, 4825–4841 (2022).

39. Barman, M. K., Sinha, A. K. & Nembenna, S. An efficient and recyclable thiourea-supported copper(i) chloride catalyst for azide–alkyne cycloaddition reactions. *Green Chem.* **18**, 2534–2541 (2016).

40. Alavinia, S., Ghorbani-Vaghei, R., Asadabadi, S. & Atrian, A. Sodium alginate/diethyleneamine-triazine-sulfonamide nanocomposite for adsorptive removal of Pb(II) and methyl violet from aqueous solutions. *Mater. Chem. Phys.* **293**, 126915 (2023).

41. Maddani, M. R. & Prabhu, K. R. A concise synthesis of substituted thiourea derivatives in aqueous medium. *J. Org. Chem.* **75**, 2327–2332 (2010).

42. Nguyen, T., Ermolenko, L. & Al-Mourabit, A. Three-component reaction between isocyanides, aliphatic amines and elemental sulfur: Preparation of thioureas under mild conditions with complete atom economy. *Synthesis (Stuttg).* **46**, 3172–3179 (2014).

43. Tan, W., Wei, J. & Jiang, X. Thiocarbonyl surrogate via combination of sulfur and chloroform for thiocarbamide and oxazolidi-nethione construction. *Org. Lett.* **19**, 2166–2169 (2017).

44. Linton, B. R., Carr, A. J., Orner, B. P. & Hamilton, A. D. A versatile one-pot synthesis of 1,3-substituted guanidines from carbamoyl isothiocyanates. *J. Org. Chem.* **65**, 1566–1568 (2000).

45. Davies, L. Environmental Health Criteria 230: Nitrobenzene. *Environmental Health Criteria* i–265 (2003).

46. Rostami-Vartooni, A., Alizadeh, M. & Bagherzadeh, M. Green synthesis, characterization and catalytic activity of natural bentonite-supported copper nanoparticles for the solvent-free synthesis of 1-substituted 1H-1,2,3,4-tetrazoles and reduction of 4-nitrophenol. *Beilstein J. Nanotechnol.* **6**, 2300–2309 (2015).

47. Jadhav, P. M. *et al.* Recent advances in nanocatalyzed synthesis of triazoles and tetrazoles and their biological studies. *Nanocatal. Synth. Bioact. Heterocycles* https://doi.org/10.1201/9781003141488-8 (2022).

48. Akbarzadeh, P., Koukabi, N. & Kolvari, E. Anchoring of triethanolamine–Cu(II) complex on magnetic carbon nanotube as a promising recyclable catalyst for the synthesis of 5-substituted 1H-tetrazoles from aldehydes. *Mol. Divers.* **24**, 319–333 (2020).

49. Zhang, Y. Y. *et al.* Palladium nanoparticles encapsuled in MOF: An efficient dual-functional catalyst to produce benzylmalononitrile derivatives by one-pot reaction. *Mol. Catal.* **518**, 112068 (2022).

50. Shekarlab, N., Ghorbani-Vaghei, R. & Alavinia, S. preparation and characterization of copper/polysulfonamide complex immobilized on geraphene oxide as a novel catalyst for the synthesis of pyrimido[1,2-a]benzimidazoles. *Appl. Organomet. Chem.* **34**, e5918 (2020).

51. Izadkhah, V. *et al.* Fabrication of zirconium metal-organic-framework/poly triazine-phosphanimine nanocomposite for dye adsorption from contaminated water: Isotherms and kinetics models. *J. Mol. Struct.* **1275**, 134691 (2023).

52. Alavinia, S. & Ghorbani-Vaghei, R. Magnetic Fe$_3$O$_4$ nanoparticles in melamine-based ternary deep eutectic solvent as a novel eco-compatible system for green synthesis of pyrido[2,3-d]pyrimidine derivatives. *J. Mol. Struct.* **1270**, 133860 (2022).

53. Natarajan, A. *et al.* Synthetic studies toward Aryl-(4-aryl-4 H -[1,2,4]triazole-3-yl)-amine from 1,3-Diarylthiourea as urea mimetics. *J. Org. Chem.* **70**, 6362–6368 (2005).

54. Zhang, Z., Wu, H.-H. & Tan, Y.-J. A simple and straightforward synthesis of phenyl isothiocyanates, symmetrical and unsymmetrical thioureas under ball milling. *RSC Adv.* **3**, 16940–16944 (2013).

55. Singh, K. & Sharma, S. An isocyanide based multi-component reaction under catalyst- and solvent-free conditions for the synthesis of unsymmetrical thioureas. *Tetrahedron Lett.* **58**, 197–201 (2017).

56. Koshti, V. S., Thorat, S. H., Gote, R. P., Chikkali, S. H. & Gonnade, R. G. The impact of modular substitution on crystal packing: the tale of two ureas. *CrystEngComm* **18**, 7078–7094 (2016).

57. Dashen, L. & Brewster, R. Q. The action of ethylene dibromide upon disubstituted thioureas. *Trans. Kansas Acad. Sci.* **40**, 103 (1937).

58. Serrano, J. L. *et al.* Synthesis and process optimization of symmetric and unsymmetric barbiturates C5-coupled with 2,1-benzisoxazoles. *Mol. Divers.* **24**, 155–166 (2020).

59. Wagh, G. D., Pathare, S. P. & Akamanchi, K. G. Sulfated-tungstate-catalyzed synthesis of ureas/thioureas via transamidation and synthesis of forchlorofenuron. *Chem. Sel.* **3**, 7049–7053 (2018).

60. Gawande, M. B. *et al.* First application of core-shell Ag@Ni magnetic nanocatalyst for transfer hydrogenation reactions of aromatic nitro and carbonyl compounds. *RSC Adv.* **3**, 1050–1054 (2013).

61. Babamoradi, J., Ghorbani-Vaghei, R. & Alavinia, S. CuI nanoparticles supported on a novel polymer-layered double hydroxide nanocomposite: An efficient heterogeneous nanocatalyst for the synthesis of bis-*N*-arylsulfonamides. *RSC Adv.* **11**, 19147–19157 (2021).

Author contributions

S.H.: Doing laboratory work and preparing data. S.A.: involved in conceptualization, methodology, resources, writing original draft, reviewing and editing, and formal analysis. R.G.-V. took part in conceptualization, investigation, supervision, writing, review, and editing.

Competing interests

The authors declare no competing interests.

Additional information

Supplementary Information The online version contains supplementary material available at https://doi.org/10.1038/s41598-023-40190-w.

Correspondence and requests for materials should be addressed to R.G.-V.

Reprints and permissions information is available at www.nature.com/reprints.

Publisher's note Springer Nature remains neutral with regard to jurisdictional claims in published maps and institutional affiliations.